

1 **Revision 2**

2 **A Machine Learning Approach to Discrimination of Igneous Rocks**  
3 **and Ore Deposits by Zircon Trace Elements**

4 Word Count: 9214

5 Zi-Hao Wen<sup>1,2,3</sup>, Lin Li<sup>3,4</sup>, Christopher L. Kirkland<sup>5</sup>, Sheng-Rong Li<sup>3,6</sup>, Xiao-Jie

6 Sun<sup>7</sup>, Jia-Li Lei<sup>8</sup>, Bo Xu<sup>1,3</sup> and Zeng-Qian Hou<sup>9</sup>

7 <sup>1</sup>*School of Gemology, China University of Geosciences, Beijing 100083, China*

8 <sup>2</sup>*Deutsches GeoForschungsZentrum GFZ, Potsdam 14473, Germany*

9 <sup>3</sup>*State Key Laboratory of Geological Processes and Mineral Resources, China*  
10 *University of Geosciences, Beijing 100083, China*

11 <sup>4</sup>*Institute of Earth Science, China University of Geosciences, Beijing 100083, China*

12 <sup>5</sup>*Timescales of Mineral Systems Group, School of Earth and Planetary Sciences,*  
13 *Curtin University, Perth 6845, Australia*

14 <sup>6</sup>*School of Earth Science and Resources, China University of Geosciences, Beijing*  
15 *100083, China*

16 <sup>7</sup>*China Telecom Co., LTD. Beijing Branch, Beijing 100010, China*

17 <sup>8</sup>*School of Earth Sciences, Zhejiang University, Hangzhou 310027, China*

18 <sup>9</sup>*Institute of Geology, Chinese Academy of Geological Sciences, Beijing 10037,*  
19 *China*

20

21 Corresponding author: Lin Li ([clark.li@cugb.edu.cn](mailto:clark.li@cugb.edu.cn))

22

23 **ABSTRACT**

24 The mineral zircon has a robust crystal structure, preserving a wealth of  
25 geological information through deep time. Traditionally, trace elements in magmatic  
26 and hydrothermal zircon have been employed to distinguish between different

27 primary igneous or metallogenic growth fluids. However, classical approaches based  
28 on mineral geochemistry are not only time-consuming, but often ambiguous due to  
29 apparent compositional overlap for different growth environments. Here, we report a  
30 compilation of 11004 zircon trace element measurements from 280 published  
31 articles, 7173 from crystals in igneous rocks and 3831 from ore deposits.  
32 Geochemical variables include Hf, Th, U, Y, Ti, Nb, Ta, and the REEs. Igneous rock  
33 types include kimberlite, carbonatite, gabbro, basalt, andesite, diorite, granodiorite,  
34 dacite, granite, rhyolite and pegmatite. Ore types include porphyry Cu-Au-Mo,  
35 skarn-type polymetallic, intrusion-related Au, skarn-type Fe-Cu, and Nb-Ta deposits.  
36 We develop Decision Tree, XGBoost and Random Forest algorithms with this zircon  
37 geochemical information to predict lithology or deposit type. The F1-score indicates  
38 that the Random Forest algorithm has the best predictive performance for  
39 classification of both lithology and deposit type. The eight most important zircon  
40 elements from the igneous rock (Hf, Nb, Ta, Th, U, Eu, Ti, Lu,) and ore deposit (Y,  
41 Eu, Hf, U, Ce, Ti, Th, Lu) classification models, yielded reliable F1-scores of 0.919  
42 and 0.891, respectively. We present a web page portal (<http://60.205.170.161:8001/>)  
43 for the classifier and employ it to a case study of Archean igneous rocks in Western  
44 Australia and ore deposits in Southwest China. The machine learning classifier  
45 successfully determines the known primary lithology of the samples, demonstrating  
46 significant promise as a classification tool, where host rock and ore deposit type is  
47 unknown.

48 **Keywords:** Zircon trace elements; igneous rocks classification; ore deposits  
49 classification; machine learning; Random Forests

50

## 51 INTRODUCTION

52 Zircon ( $\text{ZrSiO}_4$ ) is common accessory mineral which grows in most silicate  
53 rocks and in many ore deposits. Zircon trace element chemistry reflects the  
54 partitioning of elements in the melt or fluid environment and the mineral during its  
55 crystallization (or later during recrystallization). Trace elements from a melt or other  
56 fluid can replace Zr, Si, or sit within interstitial spaces and become incorporated into  
57 the crystal during magmatic growth or during later metamorphism ([Geisler et al.](#)  
58 [2007](#); [Hanchar et al. 2001](#); [Hoskin and Schaltegger, 2003](#)). Different trace elements  
59 within the zircon crystal record different information, for example the radioactive  
60 elements Th, U, and Pb can be used to calculate ages ([Lee et al. 1997](#)) but also retain  
61 crude relationships with magma fractionation state and bulk rock chemistry (e.g.  
62 [Kirkland et al. \(2015\)](#) on Th/U), Ti content is temperature dependent ([Watson et al.](#)  
63 [2006](#)), Ce and Eu content is a key parameter related to magma oxygen fugacity  
64 ([Trail et al. 2012](#)), and Nb and Ta content reflects the degree of magmatic  
65 differentiation ([Chen et al. 2021](#)). Hf readily substitutes for Zr in the zircon structure  
66 meaning that the  $^{176}\text{Hf}/^{177}\text{Hf}$  isotopic ratio, reflecting source Lu/Hf fractionation, is a  
67 powerful tool for crustal evolution studies (e.g. [Belousova et al. 2010](#)). A wide range  
68 of other geochemical parameters in zircon have been used to understand this mineral

69 and hence a rocks crystallization and later alteration history ([Bell et al. 2019](#);  
70 [Claiborne et al. 2010](#); [Olson et al. 2017](#); [Zeng et al. 2017](#)).

71 Studies on the classification of igneous rocks based on zircon compositions are  
72 abundant ([Belousova et al. 2002](#); [Breiter et al. 2014](#); [Gudelius et al. 2020](#); [Nardi et al.](#)  
73 [2013](#)). Utilizing a series of binary diagrams for zircon trace elements, [Belousova et](#)  
74 [al. \(2002\)](#) found that the content of specific elements varied between different  
75 igneous rock types. [Belousova et al. \(2002\)](#) used this information to construct a trace  
76 element Decision Tree to distinguish between potentially different igneous rocks  
77 precipitating zircon from their primary magma. Zircon composition has also been  
78 used as a pathfinder for mineralization ([Lu et al. 2019](#)), as there are differences in  
79 temperature, oxygen fugacity, water content, and magma fractionation state for  
80 barren and mineralized fluids which become encoded into zircons mineral chemistry.  
81 Porphyry-type Cu-Au-Mo deposits are commonly associated with intrusive bodies  
82 with high oxygen fugacity and water content ([Lu et al. 2016](#)). W-Sn deposits are  
83 associated with generally low oxygen fugacity ([Yang et al. 2020](#)). Nb-Ta deposits  
84 are often associated with highly evolved rocks ([Yang et al. 2014](#)). In the last 20  
85 years, LA-ICPMS (Laser Ablation – Inductively Coupled Plasma Mass  
86 Spectrometry) has become a popular tool for both geochronology and geochemical  
87 analysis of zircon, allowing large datasets to be rapidly collected from relatively  
88 small sample volumes within individual zircon crystals ([Jackson et al. 1992](#)). As  
89 more zircon data are published, there is the potential to search for patterns within

90 this “big data” and use the resulting information to address geological problems that  
91 may have lacked clear resolution with smaller datasets.

92 Machine learning is important in the context of “big data” and uses  
93 computational power to develop algorithms and statistical models to address a broad  
94 range of geological questions. With these algorithms and models, computer systems  
95 can process and analyze massive amounts of data in a short time, and make  
96 predictions or decisions on their own without explicit instructions (Mitchell 1997).  
97 Supervised learning is an important branch of machine learning, which predicts class  
98 labels by training a model. It requires input information to be labeled and divides it  
99 into a training dataset and a test dataset. The training dataset is used to teach the  
100 model and the test dataset serves to evaluate the performance of the constructed  
101 model (Hastie et al. 2009). Common supervised learning models include Decision  
102 Tree, Support Vector Machine (SVM), Random Forest, Extreme Gradient Boosting  
103 (XGBoost), and KNN. These models have already yielded some promising results  
104 for mineralogy. For example, models have been developed to predict the host rocks  
105 of quartz (Wang et al. 2021) and garnet (Schönig et al. 2021), tracing the possible  
106 provenance of detrital apatite in sedimentary rocks (O'Sullivan et al. 2020), and  
107 estimating the temperature and storage depth of clinopyroxene-bearing magma  
108 (Petrelli et al. 2020). For zircon grains, recently, Zou et al. (2022) successfully  
109 distinguished fertile and barren porphyries with the help of Random Forests and  
110 neural networks.

111           Distinct from [Zou et al. \(2022\)](#)'s study, here we aim to discriminate different  
112 magmatic rocks and different mineralizing fluids with zircon trace elements. Such  
113 classification model would have important use in provenance analysis of detrital  
114 zircon and ore prospecting. Specifically, with lithological context removed from a  
115 detrital zircon this tool may help refine provenance interpretations including  
116 lithology of the source ([Hoskin and Ireland 2000](#)), its potential geodynamic setting  
117 ([Grimes et al. 2015](#)), and expand the exploration search space for mineral systems  
118 ([Lu et al. 2016](#)). In this study, we prepared separate databases of zircon chemical  
119 composition for igneous rocks and ore deposits. We show that a Random Forests  
120 algorithm yields the best prediction for both igneous rock and ore deposit type. We  
121 also filtered the most significant elements from the compilation and developed a  
122 model using fewer variables which is able to achieve a similar classification effect.  
123 Compared with conventional methods, machine learning is both more efficient and  
124 reliable in classifying igneous rocks and ore deposits.

125

## 126                           **ZIRCON DATABASES AND CONVENTIONAL**

## 127   **CLASSIFICATION METHODS**

### 128   **Zircon databases**

129           We collected 11004 zircon trace element measurements from 280 published  
130 articles, with samples widely distributed over both space and time ([Fig. 1](#)). Part of  
131 the data is extracted from the online database

132 <https://data.goettingen-research-online.de>. The elements in the database are Hf, U,  
133 Th, Y, Ti, Nb, Ta, and REE. Although zircon also contains P, Ca, Al, Fe, Sc, and Sr,  
134 the amount of data currently available for these elements is limited and thus is not  
135 yet suitable for inclusion in this form of analysis.

136 The igneous rock or ore deposit classification and primary publication is given  
137 in **Table 1**, and detailed zircon information can be found at  
138 [https://github.com/ZihaoWen123/geology\\_class](https://github.com/ZihaoWen123/geology_class), including sample location, trace  
139 element contents and references. The Igneous Rocks Database includes nine  
140 different igneous rock types, with rock names extracted from the lithological  
141 descriptions within in the source publications. However, some of these samples have  
142 similar mineral assemblages. To improve classification efficiency, closely  
143 comparable mineral assemblages were integrated (**Table 1**). Ultimately, the Igneous  
144 Rock Database contains six discrete rock types: kimberlite, carbonatite, basic rocks  
145 (BR), intermediate rocks (IR), acid rocks (AR), and pegmatite. The Ore Deposit  
146 Database covers five discrete deposit types (**Table 1**): porphyry Cu-Au-Mo deposit,  
147 skarn-type polymetallic deposit, intrusion-related Au deposit, skarn-type Fe-Cu  
148 deposit and Nb-Ta deposit. Skarn-type polymetallic deposits in the database are  
149 mainly found in southern China and Southeast Asia, and are dominated by W, Sn,  
150 with minor Pb, Zn and Sb. Notably the above classification of igneous rocks and ore  
151 deposits is based on the description of field lithology and deposits in the published  
152 source articles.

153

## 154 **Conventional classification methods**

155 Before developing a machine learning method, we analyzed the zircon data  
156 from the igneous rocks ([Belousova et al. 2002](#); [Claiborne et al. 2010](#); [Gagnevin et al.](#)  
157 [2010](#); [Gudelius et al. 2020](#)) and ore deposits ([Large et al. 2018](#); [Lee et al. 2017](#); [Lu](#)  
158 [et al. 2016](#)) using more traditional two-dimensional classification methods (**Fig. 2**).  
159 REE depletion is regarded as an important feature of kimberlites ([Hoskin and](#)  
160 [Ireland 2000](#)). We found that not only REE (med. 299 ppm), but also Th (med. 33.5  
161 ppm), U (med. 66.9 ppm) and Y (med. 248 ppm) are depleted in zircon crystals from  
162 kimberlites. In pegmatites Nb (med. 19.4 ppm), Ta (med. 8.32 ppm), REE (med.  
163 1789ppm), U (med. 2123 ppm), Y (med. 2256 ppm) are all enriched (**Fig. 2a-c**).  
164 Niobium, Ta, and REE deposits are often associated with pegmatites ([Van](#)  
165 [Lichtervelde et al. 2009](#); [Seidler et al. 2005](#); [Zhang et al. 2004](#)), and some U deposits  
166 are found in areas which have significant pegmatite shows ([Chen et al. 2019](#)). Some  
167 Nb deposits are also spatially correlated with carbonatites ([Melgarejo et al. 2012](#);  
168 [Wu et al. 2021](#)), as Nb (med. 52.5 ppm) is also enriched in carbonatites, while Ti  
169 (med. 3.03), REE (med. 519 ppm), U (med. 31.5 ppm), Y (med. 554 ppm) are  
170 generally deficient. **Figure 4d** shows the method proposed by ([Grimes et al. 2007](#))  
171 for tracing zircon source area, which can constrain kimberlites but places few limits  
172 on the source of zircon from other rock types. The elemental contents of AR (Acid  
173 rock), IR (Intermediate rock), and BR (Basic rock) are not significantly enriched or



174 depleted and all significantly overlap and cannot be uniquely identified via bivariate  
175 plots (**Fig. 2**).

176 Relevant to deposit formation, oxygen fugacity and water content are known to  
177 be related to the transport and deposition of metals ([Wyborn et al., 1994](#)). Some  
178 studies have found that Eu and Ce anomalies in zircon are controlled by magma  
179 temperature and also the crystallization of other minerals such as titanite, plagioclase,  
180 and hornblende, in addition to oxygen fugacity ([Nathwani et al. 2021](#); [Loader et al.](#)  
181 [2022](#)). Nonetheless, exploration approaches using Eu/Eu\* ([Dilles et al. 2015](#)) and  
182 Ce\* ([Loader et al. 2017](#)) have proved useful in distinguishing fertile from barren  
183 porphyry systems ([Shen et al. 2015](#); [Shu et al. 2019](#); [Pizarro et al. 2020](#)) (**Fig. 2e**).  
184 Recent studies have found that the water content of zircon crystals can be measured  
185 directly to estimate the amount of water within the primary magma ([Xia et al. 2019](#)).  
186 Another geochemical signature in zircon, with relevance for ores, is that water-rich  
187 magmas promote hornblende crystallization that suppresses plagioclase  
188 crystallization, resulting in Eu enrichment and Y deficiency in zircon. [Lu et al. \(2016\)](#)  
189 proposed that  $\text{Eu}/\text{Eu}^*/\text{Y} \times 10000$  and  $\text{Ce}/\text{Nd}/\text{Y}$  of zircon is positively correlated with  
190 magma water content (**Fig. 2f**). We find that skarn-type polymetallic deposits are  
191 associated with low oxygen fugacity and water content environments, while  
192 porphyry-type deposits, intrusion-related Au deposits, and skarn-type Fe-Cu deposits  
193 are associated with high oxygen fugacity and water content (**Fig. e, f**). Garnet is  
194 widespread in skarn rocks, which have a greater preference for HREE ([Lee et al.](#)

195 [2017](#); [Rubatto 2002](#)). This chemical affinity may be responsible for the HREE  
196 deficit and low Yb/Gd ratios in zircons from skarn-type polymetallic deposits and  
197 skarn-type Fe-Cu deposits ([Fig. 2g](#)). In addition, zircons in Nb-Ta deposits  
198 unsurprisingly have high Nb and Ta contents ([Fig. 2h](#)).

199

## 200 **DATA PRE-PROCESSING FOR MACHINE LEARNING**

### 201 **METHODS**

202 Data pre-processing and model building was completed in Python on the  
203 scikit-learn platform ([Pedregosa et al. 2011](#)).

#### 204 **Addressing missing values – Imputation**

205 In data analysis, data integrity is very important to obtain accurate and reliable  
206 results. Therefore, filling in missing values with appropriate estimates (imputation)  
207 is an essential step in data pre-processing. There are some missing compositional  
208 values in the data set, either because the elemental content was below the detection  
209 limit of the LA-ICPMS, because the analyst simply did not collect that element, or  
210 there was some other analytical limitation imposed on the acquisition.

211 For the first missing data case, we elected to remove elements with very low  
212 contents, such as La and Pr. Lanthanum and Pr contents are often below the  
213 detection limit and measurement of these elements are susceptible to reflecting the  
214 content of mineral inclusions within the zircon grains, rather than the zircon itself.  
215 These two elements were also avoided by other researchers, for example when  
216 calculating  $Ce^{3+}$  content from rare earth elements of zircon and estimating oxygen

217 fugacity (Zhong et al. 2019). In addition, we do not consider elements with >20%  
218 missing values in the dataset. This is because estimating a large number of missing  
219 values brings a heightened degree of uncertainty and could cause the model to  
220 poorly reflect the true data distribution. Niobium and Ta in the ore deposits database  
221 suffers from a large number of missing measurements.

222 For the second and third case of missing data (elements not measured for  
223 whatever reason), we are able to use the "knn-classification" and "iterative" vacancy  
224 filling methods as there is sufficient information to estimate the missing parameter  
225 in the dataset (Emmanuel et al. 2021). The term "knn-classification" uses the known  
226 characteristics of the data points to determine the nearest K samples to the missing  
227 data according to Euclidean distance (Eqs. 1,2), and then fills the missing values by  
228 averaging the results of these K samples (Emmanuel et al. 2021).

$$229 \quad d_{xy} = \sqrt{(\text{weight} \times \text{squared distance from present coordinates})} \quad 1$$

$$230 \quad \text{weight} = (\text{Total number of coordinates}) / (\text{Number of present coordinates}) \quad 2$$

231 The alternative "iterative" method involves defining a model that predicts each  
232 missing element as a function of all other elements and repeating this process of  
233 estimating feature values multiple times (Emmanuel et al. 2021). Initially the  
234 procedure assumes that the missing data has a mean value. The concentration is then  
235 re-estimated based on the pattern within the entire dataset. The imputed values are  
236 used to update the missing values in the original data set. This repetition allows  
237 refined estimates for other features and can be used as the input in subsequent

238 iterations of predicting missing values.

239

## 240 **Data standardization**

241 Data standardization unifies the units of measure and magnitudes of different  
242 features (in our case, elements), eliminating the effects of order-of-magnitude  
243 differences and making the data more comparable. We compared different data  
244 standardization strategies, including "Min-Max", "Log" and "Z-score".

245 "Min-Max" scales the original data in the range [0,1], i.e., to map the data to  
246 the specified interval by linear transformation of the original data (**Eq 3**).

$$247 \quad x = (x_i - \min(x_i)) / (\max(x_i) - \min(x_i)) \quad 3$$

248 "Log" (log transformation) standardizes the data by taking the logarithm of the  
249 data (**Eq 4**).

$$250 \quad x = \log(x_i + 1) \quad 4$$

251 The "Z-score" transforms the data into a data structure with mean of 0 and  
252 standard deviation equal to 1 (**Eq 5**). Where  $\mu$  is the mean of the original data and  $\sigma$   
253 is the standard deviation of the original data.

$$254 \quad x = (x_i - \mu) / \sigma \quad 5$$

255

## 256 **Class imbalance**

257 In the igneous rock database, the AR lithology has the most data with 2594  
258 samples. The pegmatite lithology has the least data in the database with 218 samples  
259 (**Table 1**). In the case of the ore deposits database, the porphyry type Cu-Mo-Au  
260 deposit is the most numerous with 2122 samples and the Nb-Ta deposit is the least

261 numerous with 81 samples (**Table 1**). This imbalance in the number of samples in  
262 different classes (lithology or deposit types) could cause the model to be more  
263 inclined to predict specific classes with more data and thus perform worse on classes  
264 with less data, resulting in biased model output ([Japkowicz and Stephen 2002](#)).

265 To address the apparent class imbalance a synthetic minority over-sampling  
266 technique (SMOTE) can be used ([Chawla et al. 2002](#)). This method first calculates  
267 the distance of each data point, in a minority class, from the adjacent K data. Then a  
268 number of data points are randomly selected from the K nearest neighbors to  
269 generate a new synthetic data point. This new synthetic data point is added to the  
270 original minority class dataset, increasing its number.

271

## 272 MACHINE LEARNING METHODS

273 Data is divided into training and testing sets with the training set : testing set  
274 ratio set at 9:1. The training set was used to develop the model and for parameter  
275 tuning. The test set was used to evaluate the performance of the model ([Hastie et al.  
276 2009](#)). We developed Decision Tree ([Myles et al. 2004](#)), XGBoost ([Chen and  
277 Guestrin 2016](#)) and Random Forest ([Tin Kam Ho 1995](#); [Breiman 2001](#)) to fit the  
278 compiled data. These methods are all tree-based algorithms, which are  
279 non-parametric and work regardless of the distribution/collinearity of the input data.  
280 Other methods, such as SVM, Artificial Neural Network, and Logistic Regression,  
281 can be limited compared to tree-based algorithms on geochemical data due to a

282 constant sum effect ([Rollinson 1992](#)).

283

## 284 **Decision Tree**

285 A Decision Tree model is often regarded as "weak classifier" and the basis for  
286 building integrated algorithms such as XGBoost and Random Forest. A Decision  
287 Tree is built by constructing a tree model that outputs the possible outcomes and  
288 probabilities under different conditions. Specifically, it selects the best feature from  
289 all the features as the root node and repeats this process for the selected features  
290 until a Decision Tree is generated ([Myles et al. 2004](#)). In the tree model, the Gini  
291 coefficient (**Eq 6**) is used for feature selection ([Breiman 2001](#)).

$$292 \text{Gini}(t) = 1 - \sum_{i=0}^{c-1} p(i|t)^2 \quad 6$$

293

## 294 **XGBoost**

295 In the XGBoost algorithm the basic principle is to iteratively add Decision  
296 Trees to a model, with each tree attempting to correct the errors of the previous tree.  
297 During training, the model starts with a single Decision Tree and calculates the error  
298 (or loss) of the predictions on the training data. The algorithm then adds another  
299 Decision Tree to the model, but this time aims to correct the errors within the first  
300 Decision Tree. The combined output of both Decision Trees are then used to  
301 calculate a new error estimate, and the process repeats with additional Decision  
302 Trees added until the error is minimized. The predictions from each tree are

303 combined by adding them together to produce the final output (Chen and He 2015;  
304 Chen and Guestrin 2016).

305

### 306 **Random Forest**

307 In a Random Forest model the algorithm builds a forest of Decision Trees,  
308 where each tree is constructed using a random subset of the data and features (Fig.  
309 3). The trees are trained independently and are not correlated with each other. When  
310 making predictions, each Decision Tree in the forest is used to classify a given input,  
311 and the final prediction is made by averaging or taking the majority vote of the  
312 predictions from all the trees (Eq. 7) (Breiman, 2001). The algorithm can provide  
313 insight into the importance of each feature in the data during training by tracking the  
314 reduction in misclassification caused by each feature in each tree.

315 Equation 7 is the majority voting expression (Breiman 2001),  $H(x)$  denotes the  
316 combined classification model,  $h_i$  is the individual Decision Tree classification  
317 model  $Y$  denotes the output variable and  $I(\cdot)$  is the indicative function.

$$318 H(x) = \arg \max \sum_{i=1}^k I(h_i(x)=Y) \quad 7$$

319

### 320 **Parameter tuning and cross validation**

321 We adopt a Bayesian optimization algorithm to automatically adjust the  
322 parameters of the model (Snoek et al. 2012).

323 Five-fold cross-validation was employed to verify the reliability of the

324 classification model (Hastie et al. 2009) (Fig. 3). This computational operation  
325 divides the data into five equal parts and takes one part at a time for validation with  
326 the remainder of the data set used for training the model. This calculation was  
327 repeated five times and the average computed.

328

## 329 **RESULTS AND DISCUSSION**

### 330 **Traditional classification methods and its limitation**

331 Despite our efforts to use our knowledge of geology to distinguish between the  
332 different rocks and deposits, there are still many overlapping areas in Figure 2. We  
333 take the Y-U plot for igneous rocks and the Eu/Eu\*-Ce/Nd plot for ore deposits as  
334 examples, to calculate the accuracy of a conventional classification approach (Fig.  
335 4). To avoid altered samples and select the most representative chemistry of a rock,  
336 the highest and lowest 5% of elemental concentration data were not considered.  
337 Figures 4b and 4d show examples of BR and porphyry-type Cu-Au-Mo deposits,  
338 respectively. First, we count the number of data points within overlapping intervals  
339 and also calculate the overlap rate on the X- and Y-axes. We then subtract the  
340 product of the two overlap rates from 1, which is the accuracy of identifying an  
341 igneous rock or ore deposit. BR reveals a complete overlap with an identification  
342 rate of 0 (Fig. 4b). The porphyry type Cu-Au-Mo deposit has 151 data  
343 distinguishable on a Ce/Nd plot, giving an identification rate of only 9% (Fig. 4d).

344 In Figure 4a even the most accurate classification rate, that for pegmatite, is



345 only 64%, followed by carbonatite and kimberlite that are very similar with rates of  
346 19% and 13% prediction, respectively. AR, IR, and BR are completely  
347 undistinguished. A similar result is evident in **Figure 4c**, which completely fails to  
348 discriminate between Nb-Ta deposits and skarn-type Fe-Cu deposits. The highest  
349 classification accuracy is for intrusion-related Au deposits, at 52%. Skarn-type  
350 polymetallic deposits and porphyry-type Cu-Au-Mo deposits are similar with only  
351 11% and 9% prediction, respectively. In summary, traditional methods have  
352 generally poor performance in identifying different igneous rocks or ore deposits. It  
353 may be feasible to improve the identification of some rocks and deposits by making  
354 additional two-dimensional geochemical plots. However, such strategy will be both  
355 time consuming and may still be unable to uniquely distinguish between overlapping  
356 fields on discrimination plots and thus may lead to erroneous classifications.

357

### 358 **Machine learning model construction**

359 Before the selection of a machine learning algorithm, a lot of data  
360 pre-processing work is required, including treatment of missing values, data  
361 standardization, and addressing class imbalance. These steps aim to improve the  
362 accuracy, stability, and computational efficiency of the model. We ran the model on  
363 the compositional database with Decision Tree, XGBoost, and Random Forest  
364 algorithms and list the results in **Table 2**. Precision, recall, and F1-scores provide  
365 evaluation criteria for the classification models (see detailed description in [Nathwani](#)

366 [et al. \(2022\)](#)). The F1-score is the summed average of precision and recall, and is  
367 thus a useful summary of the function of the model. We observe that for igneous  
368 rocks and ore deposits, the best results are obtained by using the "knn-classification"  
369 method of filling in missing values, the "z-score" method for data standardization,  
370 and with "SMOTE" for class balance.

371       Improperly filling in the missing values would introduce new noisy data,  
372 increasing the uncertainty of the model, leading to biased results ([Pearson 2006](#)). In  
373 our models, "knn-classification" performs better than the "iterative" imputation  
374 method (**Table 2**). A possible reason for this observation is that the KNN algorithm  
375 is a similarity-based algorithm, and as the same sample group of data has a high  
376 similarity, so the "knn-classification" works better. A disadvantage of the "iterative"  
377 method is that it is computationally intensive. For data standardization, both  
378 classification models perform best with the "z-score". This may be because the  
379 "z-score" method can better preserve the information between features, avoid the  
380 influence of outliers, and does not change the shape of the original data. For class  
381 imbalance, "SMOTE" effectively increased the number of minority samples and  
382 improved their identification.

383       For machine learning algorithms, Random Forest performs the best for both  
384 databases no matter what data preprocessing method was used (**Table 2**). It is  
385 conceivable that the Decision Tree algorithm does not perform well because  
386 Random Forest and XGBoost are integrated algorithms and they are better at

387 handling data with a high level of dimensions (i.e. a large number of attributes  
388 within the dataset). The lower F1-score of XGBoost than Random Forest may be  
389 due to its tendency to overfit the data. Random Forest randomly selects some  
390 features in the training of each Decision Tree, avoiding possible overfitting caused  
391 by too many features.

392 Bayesian optimization is employed to parameterize the best igneous rocks and  
393 ore deposits models. It improves the predictive performance and accuracy of the  
394 model, reduces the risk of overfitting or underfitting, and improves the  
395 generalization ability of the model (Snoek et al. 2012). In **Table 3**, we list the  
396 parameter combinations (Detailed parameter tuning results in GitHub). The  
397 F1-scores of both igneous rocks and ore deposits classification models are  
398 significantly improved with the optimization, with scores of 0.963 and 0.961,  
399 respectively. The results of the five-fold cross-validation show that for Random  
400 Forest (**Table 4**) the precision of the classification models for igneous rocks and ore  
401 deposits has mean values of 0.947 and 0.897 respectively, suggesting that the  
402 classification models are both stable and reliable.

403 A confusion matrix was used to measure the performance of the classification  
404 model. We can see from **Figure 5a** that kimberlite has the highest value (0.959),  
405 followed by AR (0.938), IR (0.891), BR (0.882), carbonatite (0.87) and pegmatite  
406 (0.75). Some pegmatites are mistaken for AR (0.125), which may be due to the fact  
407 that they underwent a longer chemical evolution sharing ultimate compositional

408 affinity to AR. For the Ore Deposits Database (**Fig. 5b**), porphyry-type Cu-Au-Mo  
409 deposits (0.945) and intrusion-related Au deposits (0.95) have a better precision,  
410 followed by Nb-Ta deposits (0.909) and skarn-type polymetallic deposits (0.841),  
411 with skarn-type Fe-Cu deposits being the lowest (0.712). Skarn-type Fe-Cu deposits  
412 can be mistaken for porphyry-type Cu-Au-Mo deposits (0.076) and intrusion-related  
413 Au deposits (0.076) and polymetallic silica deposits (0.136). The lower scores may  
414 be because both skarn-type Fe-Cu deposits and skarn-type polymetallic deposits are  
415 spatially associated with the same geological environment. However, skarn-type  
416 Fe-Cu deposits prefer an oxidized and H<sub>2</sub>O-rich environment, as does porphyry-type  
417 Cu-Au-Mo deposits, and intrusion-related Au deposits ([Sun et al. 2019](#)).

418

#### 419 **Feature importance and model simplification**

420 Feature importance highlights how relevant a feature (e.g. trace elements in a  
421 zircon) is to the classification (e.g. the type of igneous rock or ore deposit).  
422 Permutation Feature Importance (PFI) is a method for assessing the importance of  
423 features ([Altmann et al. 2010](#)). It evaluates the influence of the feature on the model  
424 by randomly replacing the value of a feature ([Altmann et al. 2010](#)).

425 For the igneous rocks and ore deposits classification models, 19 and 17 (Nb, Ta  
426 missing values >20% were not included in the model) elements were taken into  
427 account, respectively. In **Figures 6** we present the importance scores of the features  
428 for the Igneous Rocks and Ore Deposits Databases, respectively. In the igneous

429 classification model Hf (0.123) is considered to be the most important, followed by  
430 Nb (0.120), Ta (0.089), Th (0.086) etc. and Sm (0) is considered to be the least  
431 important. In the deposit classification model, Y (0.119) is the most important,  
432 followed by Eu (0.097) ,Hf (0.067), U (0.067) etc. There are also some elements that  
433 are negative values, and they are usually considered to have a negative impact on the  
434 model, with Gd (-0.006) having the biggest negative impact.

435 To explore the relationship between the number of elements and the model  
436 scores, we first selected the top two most important elements and then added  
437 elements in descending order (**Figure 7**). The F1-score of the rock classification  
438 model increases from 0.612 to 0.902, while the deposit classification model  
439 increased from 0.478 to 0.851 until the 8th element was added. This is very close to  
440 the scores obtained with all elements in the Igneous Rock Database (0.914) and Ore  
441 Deposit Database (0.868). Therefore, we consider it acceptable to use the most  
442 important eight elements for the igneous rock and ore deposit classification models,  
443 respectively. Such approach aids in the decision of what trace elements to analyze in  
444 zircon when the goal is classifying the igneous rock source or ore deposits host,  
445 saving analytical time and costs, but arguably most importantly allowing element  
446 count times to be optimized to those most powerful elements for classification. From  
447 an algorithmic standpoint, using fewer elements in the final model will reduce its  
448 susceptibility to overfitting the training set (i.e. increases the signal to noise ratio).  
449 We additionally performed Bayesian optimal tuning for the simplified model (**Table**

450 3), which yielded F1-scores for igneous rock and deposit classification models of  
451 0.919 and 0.891, respectively.

452 Both the simplified igneous rock and ore deposit classification models contain  
453 Hf, Th, U, Eu, Ti, and Lu. The igneous rock model also contains Nb and Ta, whereas  
454 the ore deposit model also contains Y and Ce. From a geological perspective, the  
455 contents of Hf, Y, U, Th, Nb, Ta, and Lu are known to correlate with degree of  
456 magmatic evolution. Fluorine is typically abundant in evolved magmas and zircon  
457 crystals generated in such fluids (Breiter et al. 2006). Zr/Hf (Claiborne et al. 2006),  
458 Hf/Y (Gagnevin et al. 2010), Th/U (Claiborne et al. 2006; Gagnevin et al. 2010;  
459 Kirkland et al. 2015) and Nb/Ta (Gudelius et al. 2020) ratios also evaluate the  
460 degree of magma fractionation. Cerium and Eu have variable valences and thus  
461 estimate magma oxygen fugacity (Ballard et al. 2002; Loader et al. 2017; Zhong et  
462 al. 2019). Europium and Y in zircon may also reflect water content in the magma  
463 (Triantafyllou et al., 2022). Oxygen fugacity and water content track the migration  
464 and potential enrichment of metals in the crust (Dilles et al. 2015; Lu et al. 2016).  
465 Hence, the most important elements selected by the PFI algorithm appear  
466 geologically significant with established relationships to both magmatic evolution  
467 and ore deposit formation.

468 The classification models for igneous rocks and ore deposits, discussed above,  
469 based on the eight most important elements, is provided via a web page front end  
470 <http://60.205.170.161:8001/>. Users can select the most appropriate model for

471 classification and upload their zircon compositional data. The model outputs the  
472 counts per classification (also expressed as a percentage of the total number of  
473 samples). A detailed results spreadsheet can be downloaded which appends the  
474 classification onto the input file.

475

## 476 **Case study of igneous rocks and ore deposits classification model**

### 477 *Igneous rocks in Yilgarn Craton, western Australia*

478 In order to explore the performance of the machine learning model we apply it  
479 to a case study on magmatic zircon crystals from the Archean Yilgarn Craton of  
480 Western Australia. The Yilgarn Craton has an exposed area of about  $65 \times 10^4$  km<sup>2</sup> and  
481 is well endowed with a range of different mineral systems ([Cassidy et al. 2006](#))  
482 ([Figure 8a](#)). We consider a compilation of zircon geochemical data collected by  
483 LA-ICPMS which is paired with whole rock geochemistry ([Lu et al., 2019](#)). This  
484 dataset has been used to evaluate the zircon trace element content of barren granitic  
485 rocks to that paragenetically associated with mineralization. Zircon grains were  
486 filtered for U-Pb isotopic discordance as a means to exclude those that would have  
487 seen secondary alteration effects. The whole rock dataset has been filtered to include  
488 only samples with loss on ignition values <63 wt% and Al<sub>2</sub>O<sub>3</sub> <20 wt%. This  
489 filtering aims to exclude samples that are strongly altered or are plagioclase  
490 cumulates. Some samples were also excluded due to the effects of metamorphism.  
491 Whole-rock geochemical and zircon trace element data for 30 rocks in the Yilgarn

492 Craton ([https://github.com/ZihaoWen123/geology\\_class](https://github.com/ZihaoWen123/geology_class)) reflects primary  
493 compositions and is available to test the classification methods (see [Lu et al. 2019](#)).  
494 First, we classified these rocks using traditional methods based on whole-rock  
495 geochemistry, 12 are "granodiorite" and 18 are "granite" fields according to the TAS  
496 diagram ([Le Maitre et al 2002](#)), indicating that they are mainly intermediate-acid to  
497 acid rocks. We used the zircon trace elements from these 30 samples in the  
498 classification model and list the results with the whole-rock geochemical  
499 classification results in **Table 5** for comparison. The classification model indicates  
500 the rock type predicted by each zircon trace element analysis and can be expressed  
501 as the proportion of each rock type classified within any sample, as shown in the pie  
502 chart in **Figure 8b**. It is clear that the zircon based IR classification is dominant in  
503 the whole rock defined "granodiorite" field, and the AR classification is elevated in  
504 those defined by whole rock as "granite" (**Fig. 8b**). As with the classification results  
505 of the whole-rock geochemical measurements, the lithology classification model  
506 based on zircon trace elements correctly predicts that these igneous rocks are mainly  
507 intermediate-acid in composition. An obvious application of this approach would be  
508 to detrital zircon grains that are not in association with their primary magmatic  
509 source rock. The zircon classification model would enable a prediction on the most  
510 likely source lithology.

### 511 ***Ore deposits in Sanjiang region, southwest China***

512 The Sanjiang metallogenic belt, located in southwestern China (**Fig. 9a**), is one



513 of the most important polymetallic belts in China which includes several porphyry  
514 copper-gold and polymetallic skarn deposits (Hou et al. 2007; Xu et al. 2021). We  
515 compiled zircon compositional data (find data on  
516 [https://github.com/ZihaoWen123/geology\\_class](https://github.com/ZihaoWen123/geology_class)) from the Yangla skarn-type  
517 polymetallic deposit, the Pulang, and the Beiya porphyry-type Cu-Au deposits (Fig.  
518 9b). Zircon compositions were used to determine the deposit type following the  
519 deposit classification model discussed above. The Yangla polymetallic skarn deposit,  
520 formed in the Triassic-Early Jurassic (Wang et al. 2022). It was traditionally  
521 considered as a copper deposit, but a high-grade tungsten ore in this deposit was  
522 recently identified (Yang et al. 2023). Wang et al. (2022) studied a quartz diorite  
523 from this deposit. In Figure 9c, the deposit classification model gives predictions for  
524 three zircon populations from this quartz diorite. Skarn-type polymetallic deposits  
525 are the dominant classification, consistent with the known situation. In the same area,  
526 Pulang and Beiya are two super large porphyry-type Cu and Au deposits formed in  
527 the Early Jurassic and Eocene, respectively (Fig. 9b) (Meng et al. 2018). Zircon  
528 compositional data from Meng et al. (2018) was used in classification. Three zircon  
529 populations of the Pulang deposit and five of the Beiya deposit yielded  
530 classifications dominated by porphyry-type Cu-Au-Mo deposits (Fig. 9c). It is  
531 notable that porphyry Cu-Au-Mo deposits and skarn-type polymetallic deposits  
532 always ranked within the top two for number of classifications. In summary, the  
533 zircon composition based ore deposit classification model seems to offer a useful

534 indication of the potential mineralization type within an area.

535

536

## CONCLUSIONS

537 Here we show that traditional methods of classifying magmatic rocks and  
538 deposits using zircon trace elements is inefficient at best and at worst can lead to  
539 misclassification. Random Forest models are an efficient multi-dimensional  
540 computation algorithm, although such classification results are difficult to show in  
541 the form of a flow chart. Many Decision Trees are computed independently, which  
542 can save computation time. Even if we use only the most important eight elements  
543 to predict igneous rock and ore deposit types, this limited compositional information  
544 still enables good classification. A case study of igneous rocks in the Yilgarn Craton  
545 and ore deposits in the Sanjiang region demonstrates that the zircon classifier has its  
546 own unique advantages in terms of ease of use and accuracy. It offers significant  
547 potential for tracing the origin of detrital zircon grains and enhancing exploration  
548 search space by indicating metallogenic fluids.

549

550

## IMPLICATIONS

551 Zircon is a stable mineral that can preserve primary geological information and  
552 previous studies have confirmed that trace elements in this mineral are effective for  
553 tracing the origin of both igneous rocks and ore deposits. With large compilations of  
554 trace element data in zircon machine learning offers an attractive proposition to

555 classifying igneous rocks and ore deposits source based on grain chemistry. Here we  
556 collect 7173 zircon chemical data from 11 different igneous rock types and 3831  
557 analyses of 5 deposit types, worldwide. Based on this computational approach we  
558 identify the 8 most important zircon trace elements that influence zircon  
559 classification in igneous rocks and ore deposits. We then build classification models  
560 for both igneous rocks and ore deposits and validate their reliability. In addition, a  
561 web page portal (<http://60.205.170.161:8001/>) has been developed for the two  
562 (igneous / deposit) classification models. The approach is applied to a case study of  
563 zircon from known rock types in 30 igneous plutons from Western Australia.  
564 Classification models of igneous rocks and ore deposits using zircon chemical data  
565 will be clearly useful in tracing the provenance of detrital zircon grains and in  
566 reducing exploration risk by increasing the deposit halo in detrital zircon sampling  
567 surveys.

568

569

## ACKNOWLEDGEMENTS

570 This work is supported by the National Natural Science Foundation of China  
571 (Grant no. 42202084, 4222304, 91962101, 41603063, 41872038 and IGCP-662) and  
572 DDE Big Science Program. This is the 16th contribution of Bo Xu for National  
573 Mineral Rock and Fossil Specimens Resource Center. We thank Dr. Ci-Jian Yang of  
574 the Deutsches GeoForschungsZentrum, Dr. Zhangzhou J. of Zhejiang University,  
575 and Dr. Liu Haiming of the Chinese Academy of Geological Science for

576 constructive comments. We also thank Chetan L. Nathwani and an anonymous  
577 reviewer for comments that improved this work.

578

579

## REFERENCE

- 580 Altmann, A., Toloşi, L., Sander, O., and Lengauer, T. (2010) Permutation  
581 importance: A corrected feature importance measure. *Bioinformatics*, 26,  
582 1340–1347.
- 583 Bell, E.A., Boehnke, P., Barboni, M., and Harrison, T.M. (2019) Tracking chemical  
584 alteration in magmatic zircon using rare earth element abundances. *Chemical*  
585 *Geology*, 510, 56–71.
- 586 Belousova, E.A., Griffin, W.L., O'Reilly, S.Y., and Fisher, N.I. (2002) Igneous  
587 zircon: Trace element composition as an indicator of source rock type.  
588 *Contributions to Mineralogy and Petrology*, 143, 602–622.
- 589 Belousova, E.A., Kostitsyn, Y.A., Griffin, W.L., Begg, G.C., O'Reilly, S.Y., and  
590 Pearson, N.J. (2010) The growth of the continental crust: Constraints from  
591 zircon Hf-isotope data. *Lithos*, 119, 457–466.
- 592 Breiter, K., Lamarão, C.N., Borges, R.M.K., and Dall'Agnol, R. (2014) Chemical  
593 characteristics of zircon from A-type granites and comparison to zircon of  
594 S-type granites. *Lithos*, 192–195, 208–225.
- 595 Cassidy, K.F., Champion, D.C., Krapez, B., Barley, M.E., Brown, S.J.A., Blewett,  
596 R.S., Groenewald, P.B., and Tyler, I.M. (2006) A revised geological framework  
597 for the Yilgarn Craton, Western Australia, 8pp p. Western Australia Geological  
598 Survey.
- 599 Chawla, N.V., Bowyer, K.W., Hall, L.O., and Kegelmeyer, W.P. (2002) Smote:  
600 synthetic minority over-sampling technique. *Journal of Artificial Intelligence*  
601 *Research*, 16, 321–357.
- 602 Chen, T., and Guestrin, C. (2016) XGBoost: A Scalable Tree Boosting System. In In

- 603 Kdd '16: Proceedings of the 22nd ACM SIGKDD Inter- national Conference  
604 on Knowledge Discovery and data mining pp. 785–794. Association for  
605 Computing Machinery.
- 606 Chen, T., and He, T. (2015) xgboost: eXtreme Gradient Boosting. R package version  
607 04-2.
- 608 Chen, W., Zhang, G., Ruan, M., Wang, S., and Xiong, X. (2021) Genesis of  
609 Intermediate and Silicic Arc Magmas Constrained by Nb/Ta Fractionation.  
610 Journal of Geophysical Research: Solid Earth, 126, 1–15.
- 611 Chen, Y., Hu, R., Bi, X., and Luo, J. (2019) Genesis of the Guangshigou  
612 pegmatite-type uranium deposit in the North Qinling Orogenic Belt, China. Ore  
613 Geology Reviews, 115, 103165.
- 614 Claiborne, L.L., Miller, C.F., and Wooden, J.L. (2010) Trace element composition  
615 of igneous zircon: A thermal and compositional record of the accumulation and  
616 evolution of a large silicic batholith, Spirit Mountain, Nevada. Contributions to  
617 Mineralogy and Petrology, 160, 511–531.
- 618 Dilles, J.H., Kent, A.J.R., Wooden, J.L., Tosdal, R.M., Koleszar, A., Lee, R.G., and  
619 Farmer, L.P. (2015) Zircon compositional evidence for sulfur-degassing from  
620 ore-forming arc magmas. Economic Geology, 110, 241–251.
- 621 Emmanuel, T., Maupong, T., Mpoeleng, D., Semong, T., Mphago, B., and Tabona,  
622 O. (2021) A survey on missing data in machine learning. Journal of Big Data,  
623 8.
- 624 Gagnevin, D., Daly, J.S., and Kronz, A. (2010) Zircon texture and chemical  
625 composition as a guide to magmatic processes and mixing in a granitic  
626 environment and coeval volcanic system. Contributions to Mineralogy and  
627 Petrology, 159, 579–596.
- 628 Geisler, T., Schaltegger, U., and Tomaschek, F. (2007) Re-equilibration of zircon in  
629 aqueous fluids and melts. Elements, 3, 43–50.
- 630 Grimes, C.B., John, B.E., Kelemen, P.B., Mazdab, F.K., Wooden, J.L., Cheadle,

- 631 M.J., Hanghøj, K., and Schwartz, J.J. (2007) Trace element chemistry of  
632 zircons from oceanic crust: A method for distinguishing detrital zircon  
633 provenance. *Geology*, 35, 643–646.
- 634 Grimes, C.B., Wooden, J.L., Cheadle, M.J., and John, B.E. (2015) “Fingerprinting”  
635 tectono-magmatic provenance using trace elements in igneous zircon.  
636 *Contributions to Mineralogy and Petrology*, 170, 1–26.
- 637 Gudelius, D., Zeh, A., and Wilson, A.H. (2020) Zircon formation in mafic and felsic  
638 rocks of the Bushveld Complex, South Africa: Constraints from composition,  
639 zoning, Th/U ratios, morphology, and modelling. *Chemical Geology*, 546,  
640 119647.
- 641 Hanchar, J.M., Finch, R.J., Hoskin, P.W.O., Watson, E.B., Cherniak, D.J., and  
642 Mariano, A.N. (2001) Rare earth elements in synthetic zircon: Part 1. Synthesis,  
643 and rare earth element and phosphorus doping. *American Mineralogist*, 86,  
644 667–680.
- 645 Hastie, T., Tibshirani, R., and Friedman, J. (2009) *The Elements of Statistical*  
646 *Learning: Data Mining, Inference, and Prediction*, 762 p. Springer.
- 647 Hoskin, P.W.O., and Ireland, T.R. (2000) Rare earth element chemistry of zircon  
648 and its use as a provenance indicator. *Geology*, 28, 627–630.
- 649 Hoskin, P.W.O., and Schaltegger, U. (2003) The composition of zircon and igneous  
650 and metamorphic petrogenesis. *Reviews in Mineralogy and Geochemistry*, 53,  
651 27–62.
- 652 Hou, Z., Zaw, K., Pan, G., Mo, X., Xu, Q., Hu, Y., and Li, X. (2007) Sanjiang  
653 Tethyan metallogenesis in S.W. China: Tectonic setting, metallogenic epochs  
654 and deposit types. *Ore Geology Reviews*, 31, 48–87.
- 655 Jackson, S.E., Longerich, H.P., Dunning, G.R., and Fryer, B.J. (1992) The  
656 application of laser-ablation microprobe - inductively coupled plasma-mass  
657 spectrometry (LAM-ICP-MS) to in situ trace-element determinations in  
658 minerals. *Canadian Mineralogist*, 30, 1049–1064.

- 659 Japkowicz, N., and Stephen, S. (2002) The class imbalance problem: A systematic  
660 study. *Intelligent Data Analysis*, 6, 429–449.
- 661 Kirkland, C.L., Smithies, R.H., Taylor, R.J.M., Evans, N., and McDonald, B. (2015)  
662 Zircon Th/U ratios in magmatic environs. *Lithos*, 212–215, 397–414.
- 663 Large, S.J.E., Von Quadt, A., Wotzlaw, J.F., Guillong, M., and Heinrich, C.A. (2018)  
664 Magma evolution leading to porphyry Au-Cu mineralization at the Ok Tedi  
665 deposit, Papua New Guinea: Trace element geochemistry and high-precision  
666 geochronology of igneous zircon. *Economic Geology*, 113, 39–61.
- 667 Le Maitre, R.W. (2002). *Igneous Rocks: a Classification and Glossary of Terms:*  
668 *Recommendations of the International Union of Geological Sciences*  
669 *Subcommission on the Systematics of Igneous Rocks*. Cambridge University  
670 Press, Cambridge. 236 pp.
- 671 Lee, J.K.W., Williams, I.S., and Ellis, D.J. (1997) Pb, U and Th diffusion in natural  
672 zircon. *Nature*, 390, 159–162.
- 673 Lee, R.G., Dilles, J.H., Tosdal, R.M., Wooden, J.L., and Mazdab, F.K. (2017)  
674 Magmatic evolution of granodiorite intrusions at the El Salvador porphyry  
675 copper deposit, Chile, based on trace element composition and U/Pb age of  
676 zircons. *Economic Geology*, 112, 245–273.
- 677 Loader, M.A., Wilkinson, J.J., and Armstrong, R.N. (2017) The effect of titanite  
678 crystallisation on Eu and Ce anomalies in zircon and its implications for the  
679 assessment of porphyry Cu deposit fertility. *Earth and Planetary Science*  
680 *Letters*, 472, 107–119.
- 681 Loader, M.A., Nathwani, C.L., Wilkinson, J.J., and Armstrong, R.N. (2022)  
682 Controls on the magnitude of Ce anomalies in zircon. *Geochimica et*  
683 *Cosmochimica Acta*, 328, 242–257.
- 684 Lu, Y., Loucks, R.R., Fiorentini, M., Mccuaig, T.C., Evans, N.J., Yang, Z., Hou, Z.,  
685 Kirkland, C.L., Parra-avila, L.A., and Kobussen, A. (2016) Zircon  
686 Compositions as a Pathfinder for Porphyry Cu ± Mo ± Au Deposits. *Economic*

- 687           Geology Special Publication, 19, 329–347.
- 688   Lu, Y., Evans, N., and Campbell McCuaig, T. (2019) Zircon fingerprinting of  
689           magmatic-hydrothermal systems in the Archean Yilgarn Craton, 1–22 p.
- 690   Melgarejo, J.C., Costanzo, A., Bambi, A.C.J.M., Gonçalves, A.O., and Neto, A.B.  
691           (2012) Subsolidus processes as a key factor on the distribution of Nb species in  
692           plutonic carbonatites: The Tchivira case, Angola. *Lithos*, 152, 187–201.
- 693   Meng, X., Mao, J., Zhang, C., Zhang, D., and Liu, H. (2018) Melt recharge, f O<sub>2</sub>-T  
694           conditions, and metal fertility of felsic magmas: zircon trace element chemistry  
695           of Cu-Au porphyries in the Sanjiang orogenic belt, southwest China.  
696           *Mineralium Deposita*, 53, 649–663.
- 697   Mitchell, T.M. (1997) *Machine Learning*, 264 p. McGraw-Hill.
- 698   Myles, A.J., Feudale, R.N., Liu, Y., Woody, N.A., and Brown, S.D. (2004) An  
699           introduction to decision tree modeling. *Journal of Chemometrics*, 18, 275–285.
- 700   Nardi, L.V.S., Formoso, M.L.L., Müller, I.F., Fontana, E., Jarvis, K., and Lamarão,  
701           C. (2013) Zircon/rock partition coefficients of REEs, Y, Th, U, Nb, and Ta in  
702           granitic rocks: Uses for provenance and mineral exploration purposes.  
703           *Chemical Geology*, 335, 1–7.
- 704   Nathwani, C.L., Simmons, A.T., Large, S.J.E., Wilkinson, J.J., Buret, Y., and  
705           Ihlenfeld, C. (2021) From long-lived batholith construction to giant porphyry  
706           copper deposit formation: petrological and zircon chemical evolution of the  
707           Quellaveco District, Southern Peru. *Contributions to Mineralogy and Petrology*,  
708           176.
- 709   Nathwani, C.L., Wilkinson, J.J., Fry, G., Armstrong, R.N., Smith, D.J., and Ihlenfeld,  
710           C. (2022) Machine learning for geochemical exploration: classifying  
711           metallogenic fertility in arc magmas and insights into porphyry copper deposit  
712           formation. *Mineralium Deposita*, 57, 1143–1166.
- 713   O’Sullivan, G., Chew, D., Kenny, G., Henrichs, I., and Mulligan, D. (2020) The  
714           trace element composition of apatite and its application to detrital provenance



- 715 studies. *Earth-Science Reviews*, 201, 103044.
- 716 Olson, N.H., Dilles, J.H., Kent, A.J.R., and Lang, J.R. (2017) Geochemistry of the  
717 Cretaceous Kaskanak Batholith and genesis of the Pebble porphyry Cu-Au-Mo  
718 deposit, Southwest Alaska. *American Mineralogist*, 102, 1597–1621.
- 719 Pearson, R.K. (2006) The problem of disguised missing data. *ACM SIGKDD*  
720 *Explorations Newsletter*, 8, 83–92.
- 721 Pedregosa, F., Varoquaux, G., Gramfort, A., Michel, V., Thirion, B., Grisel, O.,  
722 Blondel, M., Prettenhofer, P., Weiss, R., Dubourg, V., and others (2011)  
723 Scikit-learn: Machine learning in Python. *Journal of Machine Learning*  
724 *Research*, 12, 2825–2830.
- 725 Petrelli, M. (2021) *Introduction to Python in Earth Science Data Analysis*, 229 p.  
726 Springer Textbooks in Earth Sciences, Geography and Environment. Springer  
727 International Publishing.
- 728 Petrelli, M., Caricchi, L., and Perugini, D. (2020) Machine Learning  
729 Thermo-Barometry: Application to Clinopyroxene-Bearing Magmas. *Journal of*  
730 *Geophysical Research: Solid Earth*, 125.
- 731 Pizarro, H., Campos, E., Bouzari, F., Rouse, S., Bissig, T., Gregoire, M., and  
732 Riquelme, R. (2020) Porphyry indicator zircons (PIZs): Application to  
733 exploration of porphyry copper deposits. *Ore Geology Reviews*, 126, 103771.
- 734 Rollinson, H.R. (1992) Another look at the constant sum problem in geochemistry.  
735 *Mineralogical Magazine*, 56, 469–475.
- 736 Rubatto, D. (2002) Zircon trace element geochemistry: Partitioning with garnet and  
737 the link between U-Pb ages and metamorphism. *Chemical Geology*, 184, 123–  
738 138.
- 739 Schönig, J., von Eynatten, H., Tolosana-Delgado, R., and Meinhold, G. (2021)  
740 Garnet major-element composition as an indicator of host-rock type: a machine  
741 learning approach using the Random Forest classifier. *Contributions to*  
742 *Mineralogy and Petrology*, 176, 1–21.

- 743 Seidler, J.K., Lentz, D.R., Hall, D.C., and Susak, N. (2005) Zircon-rich Ta-Nb-REE  
744 mineralization in the McKeel Lake pegmatite-aplite system, Welsford intrusion,  
745 southwestern New Brunswick. *Exploration and Mining Geology*, 14, 79–84.
- 746 Shen, P., Hattori, K., Pan, H., Jackson, S., and Seitmuratova, E. (2015) Oxidation  
747 condition and metal fertility of granitic magmas: Zircon trace-element data  
748 from porphyry Cu deposits in the central Asian orogenic belt. *Economic  
749 Geology*, 110, 1861–1878.
- 750 Shu, Q., Chang, Z., Lai, Y., Hu, X., Wu, H., Zhang, Y., Wang, P., Zhai, D., and  
751 Zhang, C. (2019) Zircon trace elements and magma fertility: insights from  
752 porphyry (-skarn) Mo deposits in NE China. *Mineralium Deposita*, 645–656.
- 753 Snoek, J., Larochelle, H., and Adams, R.P. (2012) Practical Bayesian Optimization  
754 of Machine Learning Algorithms. *Advances in neural information processing  
755 systems*.
- 756 Tin Kam Ho (1995) Random Decision Forests Tin Kam Ho Perceptron training.  
757 *Proceedings of 3rd International Conference on Document Analysis and  
758 Recognition*, 278–282.
- 759 Trail, D., Bruce Watson, E., and Tailby, N.D. (2012) Ce and Eu anomalies in zircon  
760 as proxies for the oxidation state of magmas. *Geochimica et Cosmochimica  
761 Acta*, 97, 70–87.
- 762 Triantafyllou, A., Ducea, M.N., Jepson, G., Hernández-Montenegro, J.D., Bisch, A.,  
763 and Ganne, J. (2023) Europium anomalies in detrital zircons record major  
764 transitions in Earth geodynamics at 2.5 Ga and 0.9 Ga. *Geology*, 51, 141–145.
- 765 Van Lichtervelde, M., Melcher, F., and Wirth, R. (2009) Magmatic vs. hydrothermal  
766 origins for zircon associated with Tantalum mineralization in the Tanco  
767 pegmatite, Manitoba, Canada. *American Mineralogist*, 94, 439–450.
- 768 Wang, X., Li, B., Tang, G., Lei, Z., and Chang, H. (2022) Petrogenesis and  
769 Metallogenesis of Granitoids in the Yangla Cu-W Polymetallic Deposit,  
770 Southwest China: Evidence from Zircon Trace Elements and Hf Isotope.

- 771 Minerals, 12.
- 772 Wang, Y., Qiu, K.F., Müller, A., Hou, Z.L., Zhu, Z.H., and Yu, H.C. (2021)
- 773 Machine Learning Prediction of Quartz Forming-Environments. *Journal of*
- 774 *Geophysical Research: Solid Earth*, 126, 1–11.
- 775 Watson, E.B., Wark, D.A., and Thomas, J.B. (2006) Crystallization thermometers
- 776 for zircon and rutile. *Contributions to Mineralogy and Petrology*, 151, 413–433.
- 777 Wu, B., Hu, Y.Q., Bonnetti, C., Xu, C., Wang, R.C., Zhang, Z.S., Li, Z.Y., and Yin,
- 778 R. (2021) Hydrothermal alteration of pyrochlore group minerals from the
- 779 Miaoya carbonatite complex, central China and its implications for Nb
- 780 mineralization. *Ore Geology Reviews*, 132, 104059.
- 781 Wyborn, L.A.I., Heinrich, C.A., and Jaques, A.L. (1994) Australian Proterozoic
- 782 mineral systems: Essential ingredients and mappable criteria: Proceedings of
- 783 the Australasian Institute of Mining and Metallurgy. In *The AusIMM Annual*
- 784 *Conference*. Darwin.
- 785 Xia, X.P., Cui, Z.X., Li, W., Zhang, W.F., Yang, Q., Hui, H., and Lai, C.K. (2019)
- 786 Zircon water content: Reference material development and simultaneous
- 787 measurement of oxygen isotopes by SIMS. *Journal of Analytical Atomic*
- 788 *Spectrometry*, 34, 1088–1097.
- 789 Xu, B., Hou, Z.Q., Griffin, W.L., Lu, Y., Belousova, E., Xu, J.F., and O'Reilly, S.Y.
- 790 (2021) Recycled volatiles determine fertility of porphyry deposits in collisional
- 791 settings. *American Mineralogist*, 106, 656–661.
- 792 Yang, W.B., Niu, H.C., Shan, Q., Sun, W.D., Zhang, H., Li, N.B., Jiang, Y.H., and
- 793 Yu, X.Y. (2014) Geochemistry of magmatic and hydrothermal zircon from the
- 794 highly evolved Baerzhe alkaline granite: Implications for Zr-REE-Nb
- 795 mineralization. *Mineralium Deposita*, 49, 451–470.
- 796 Yang, J.H., Zhou, M.F., Hu, R.Z., Zhong, H., Williams-Jones, A.E., Liu, L., Zhang,
- 797 X.C., Fu, Y.Z., and Mao, W. (2020) Granite-Related Tin Metallogenic Events
- 798 and Key Controlling Factors in Peninsular Malaysia, Southeast Asia: New

- 799        Insights from Cassiterite U-Pb Dating and Zircon Geochemistry. *Economic*  
800        *Geology*, 115, 581–601.
- 801    Yang, X., Wang, X., Li, B., Liu, Y., Liu, C., Liu, F., Huang, Z., and Hu, P. (2023)  
802        Discovery of tungsten orebody in the depth of the Yangla large Cu deposit,  
803        northwest Yunnan. *Acta Mineralogical Sinica*, 43, 93-96 (In Chinese with  
804        English abstract).
- 805    Zeng, L.J., Niu, H.C., Bao, Z.W., and Yang, W.B. (2017) Chemical lattice  
806        expansion of natural zircon during the magmatic-hydrothermal evolution of  
807        A-type granite. *American Mineralogist*, 102, 655–665.
- 808    Zhang, A.C., Wang, R.C., Hu, H., Zhang, H., Zhu, J.C., and Chen, X.M. (2004)  
809        Chemical evolution of Nb-Ta oxides and zircon from the Koktokay No. 3  
810        granitic pegmatite, Altai, northwestern China. *Mineralogical Magazine*, 68,  
811        739–756.
- 812    Zhong, S., Seltmann, R., Qu, H., and Song, Y. (2019) Characterization of the zircon  
813        Ce anomaly for estimation of oxidation state of magmas: a revised Ce/Ce\*  
814        method. *Mineralogy and Petrology*, 113, 755–763.
- 815    Zhu, J.J., Hu, R., Richards, J.P., Bi, X., and Zhong, H. (2015) Genesis and  
816        magmatic-hydrothermal evolution of the Yangla Skarn Cu Deposit, Southwest  
817        China. *Economic Geology*, 110, 631–652.
- 818    Zou, S., Chen, X., Brzozowski, M.J., Leng, C., and Xu, D. (2022) Application of  
819        Machine Learning to Characterizing Magma Fertility in Porphyry Cu Deposits.  
820        *Journal of Geophysical Research: Solid Earth*, 127, 1–17.

821

## FIGURE CAPTIONS

822 **FIGURE 1.** World map with sample positions labelled.

823

824 **FIGURE 2.** Zircon trace element scatter plot. (a-d) zircons collected from igneous  
825 rocks; (a) Y vs. U; (b) Th vs. U; (c) Nb vs. U; (d) U/Yb vs. Y; (e-h) zircons collected  
826 from ore deposits; (e) Eu/Eu\* vs. Ce/Nd; (f) Eu/Eu\* vs. Yb/Gd; (g)  
827 Eu/Eu\*/Y×10000 vs. Ce/Nd/Y; (h) Nb vs. Ta.

828

829 **FIGURE 3.** Cartoon of the workflow. For data pre-processing, we perform missing  
830 value processing, data normalization and data balancing for magmatic rocks and  
831 deposits database. The purple boxes denote the optimal method. For the machine  
832 learning model, Random Forest works best, and the cartoon image is put here for  
833 easy understanding. Parameter tuning and 5-fold cross-validation were also done for  
834 the model.

835

836 **FIGURE 4.** Interval graphs for calculating the accuracy of conventional  
837 classification. (a) Y vs. U plot of igneous rocks; (b) The case of BR; (c) Eu/Eu\* vs.  
838 Ce/Nd plot of ore deposits; (d) The case of porphyry-type Cu-Au-Mo deposit.  
839 Accuracy =  $1 - P(X) \times P(Y)$ , P(X) and P(Y) means the ratio of overlapping data on the  
840 X- and Y-axis.

841

842 **FIGURE 5.** Confusion matrix plot for the testing set using Random Forest. (a) Data  
843 from Igneous Rocks Database; (b) Data from Ore Deposit Database. The data in the  
844 table represents the precision of prediction (**Eq. 7**). Each column in the matrix  
845 represents the predicted category, while each row represents the true category of the  
846 data. The sum of the scores in each column is 1.

847

848 **FIGURE 6.** Ranking of feature importance using Random Forest. (a) Based on  
849 Igneous Rocks Database; (b) Based on Ore Deposit Database.

850

851 **FIGURE 7.** Trend curve of F1-score with increasing number of features using  
852 Random Forest. Element symbols are listed in descending order of feature  
853 importance in the table. Colored element symbols indicate that they are decisive for  
854 classification and can be used to simplify the model.

855

856 **FIGURE 8.** Case study of igneous rocks in Yilgarn Craton, western Australia. (a)  
857 Geological map of Yilgarn Craton with sampling points; (b) The predicted results of  
858 zircon compositions on rock samples, the division of “granite” and “granodiorite”  
859 is based on the TAS rock classification proposed by [Le Maitre \(2002\)](#).

860

861 **Figure 9.** Case study of ore deposits in Sanjiang region, southwest China. (a)  
862 Geological map showing the location of Sanjiang region ([Zhu et al. 2015](#)); (b)

863 Tectonic framework of the Sanjiang region in southwest China showing the major  
864 terranes, suture zones, arc volcanic belts, and locations of the Yangla polymetallic  
865 skarn deposit, Pulang Cu porphyry deposit and Beiya Au-Cu porphyry deposit (Zhu  
866 et al. 2015); (c) Pie chart of the classification results of ore deposits based on zircon  
867 populations. Zircon samples 45-R1, 3250-41Lb1, 3250-41Lb1 were selected from  
868 quartz diorite at the Yangla deposit (Wang et al. 2022); sample PL01 and PL 02 were  
869 selected from a quartz diorite porphyry and sample PL03 was selected from a quartz  
870 monzonite porphyry at the Pulang deposit (Meng et al. 2018); sample BY01 and  
871 BY04 were selected from a quartz monzonite porphyry and BY02, BY03, and BY05  
872 were selected from quartz syenite porphyry at the Beiya deposit (Meng et al. 2018).

873

874

## APPENDIX AND WEB PORTAL

875 To train models and validate the applicability of models in machine learning, this  
876 study collated a large amount of data. These data are peer-reviewed and published  
877 and the program code for the zircon classification model is made publicly available  
878 at ([https://github.com/ZihaoWen123/geology\\_class](https://github.com/ZihaoWen123/geology_class)). Furthermore, to aid users we  
879 have developed a website front end for the zircon classification model which should  
880 facilitate ease of use (<http://60.205.170.161:8001/>).

Figure 1

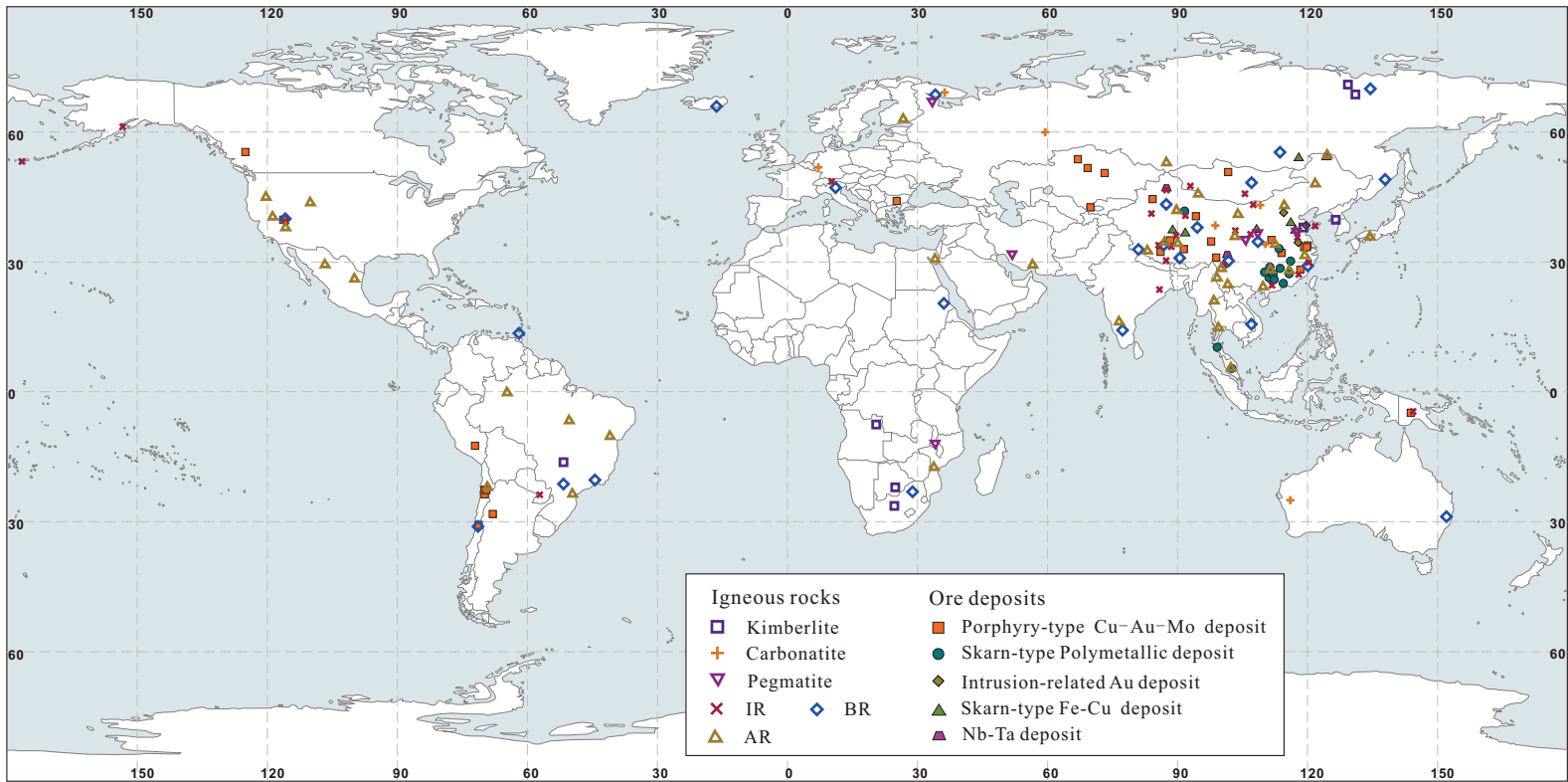




## Figure 2

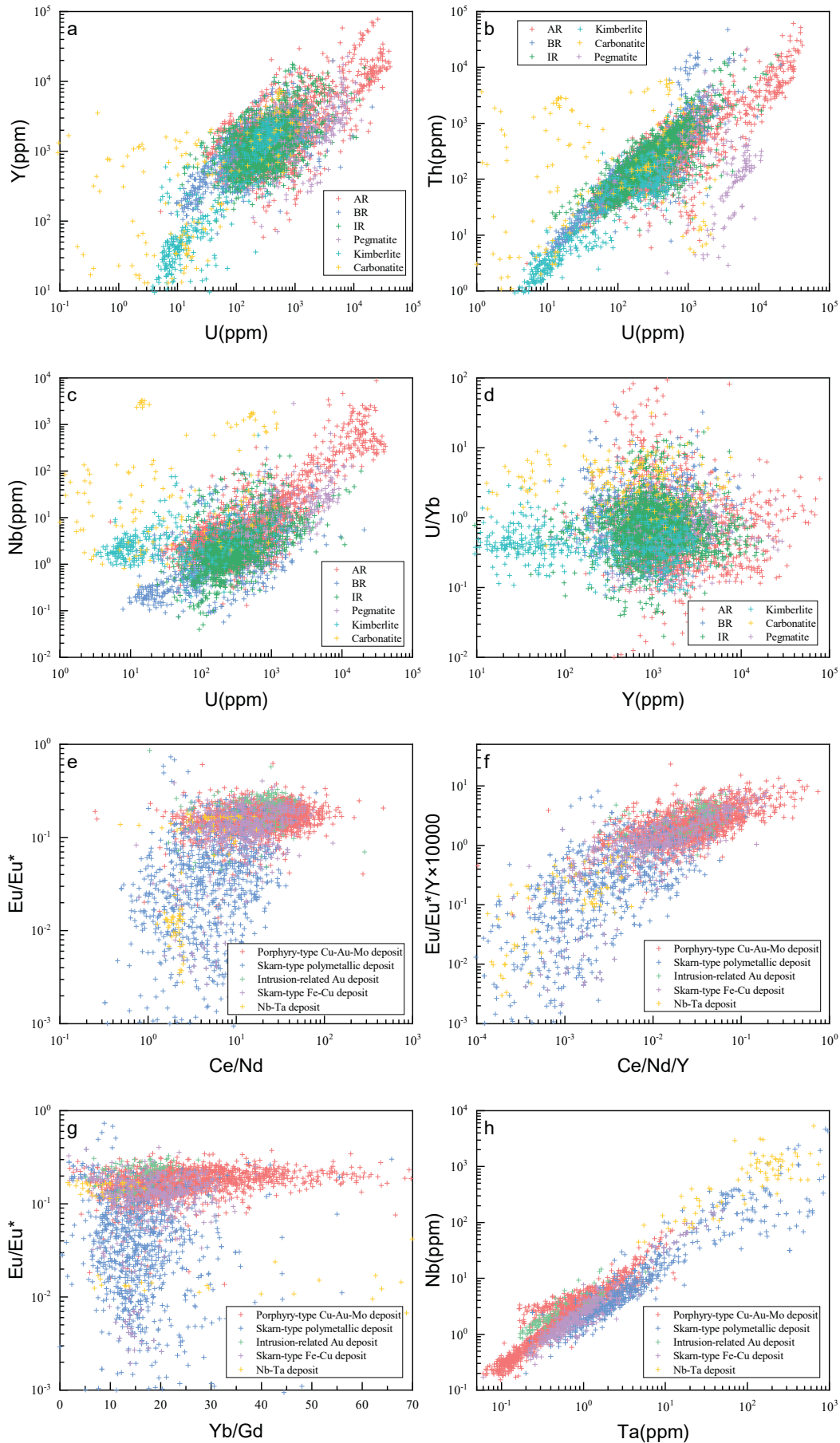


Figure 3

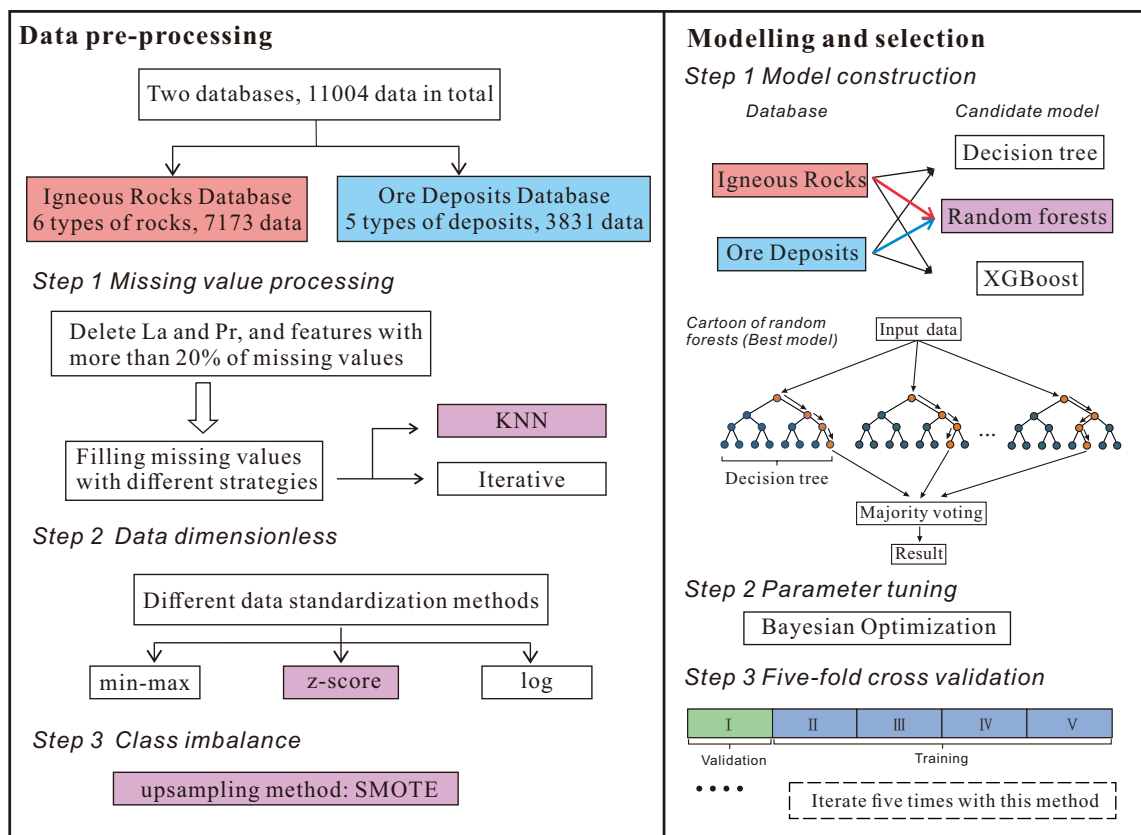


Figure 4

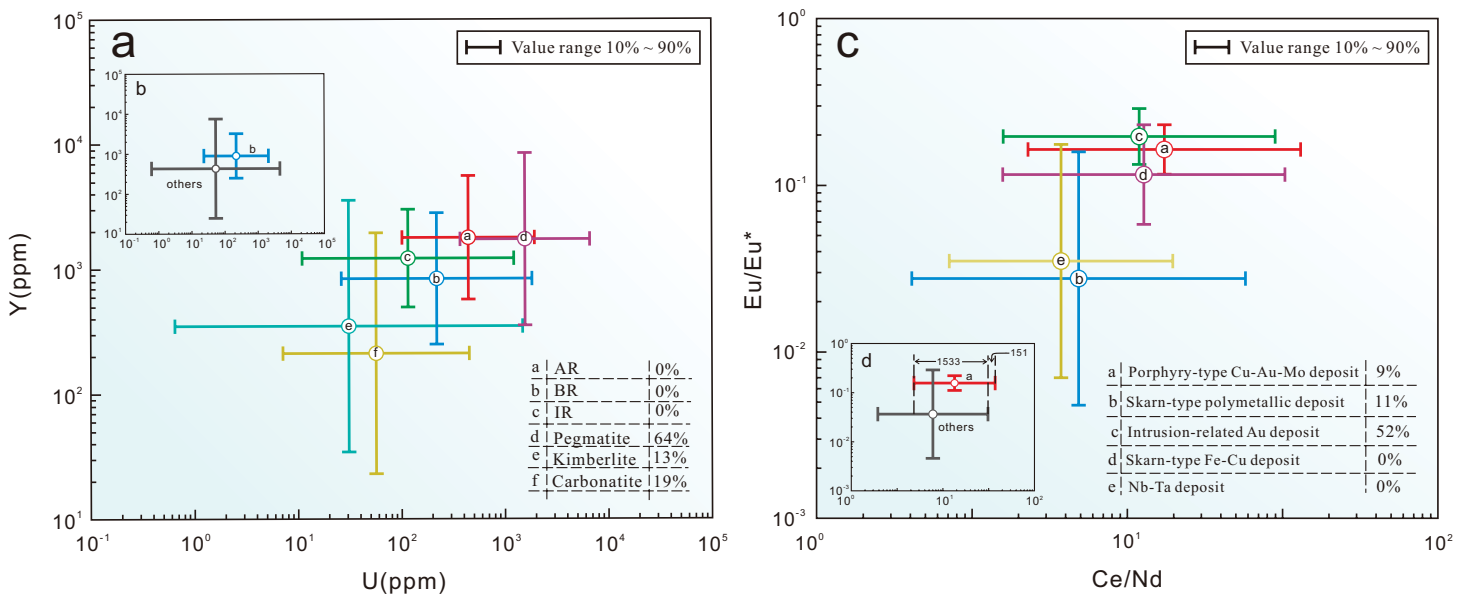


Figure 5

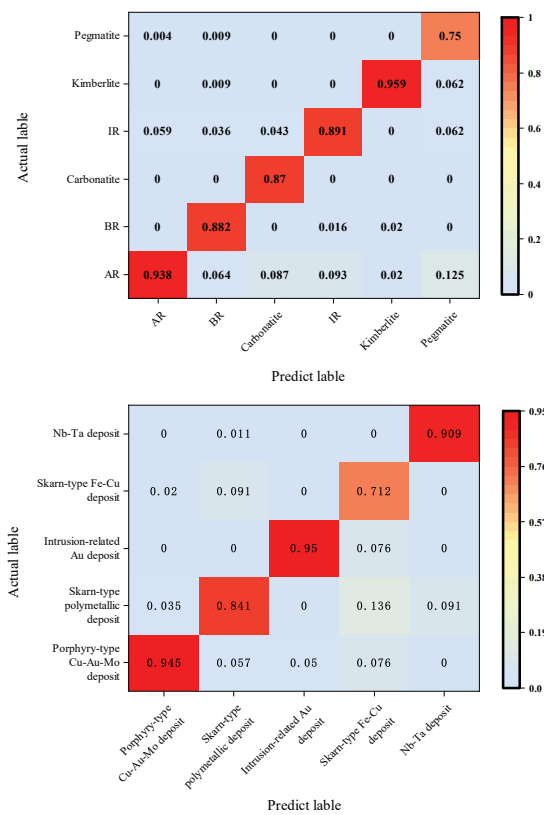


Figure 6

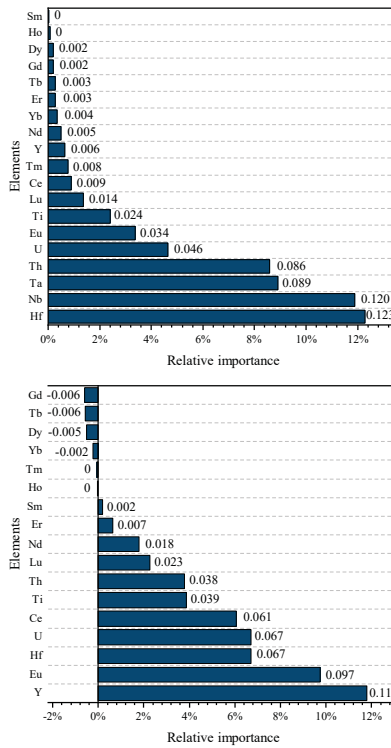


Figure 7

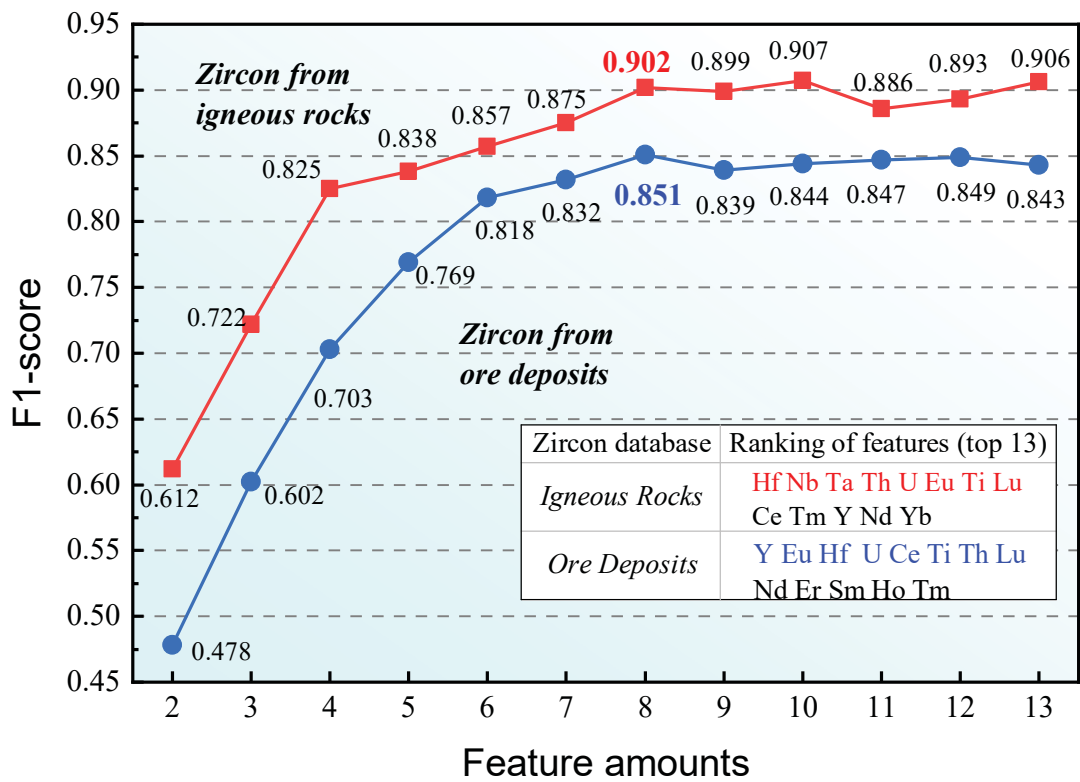


Figure 8

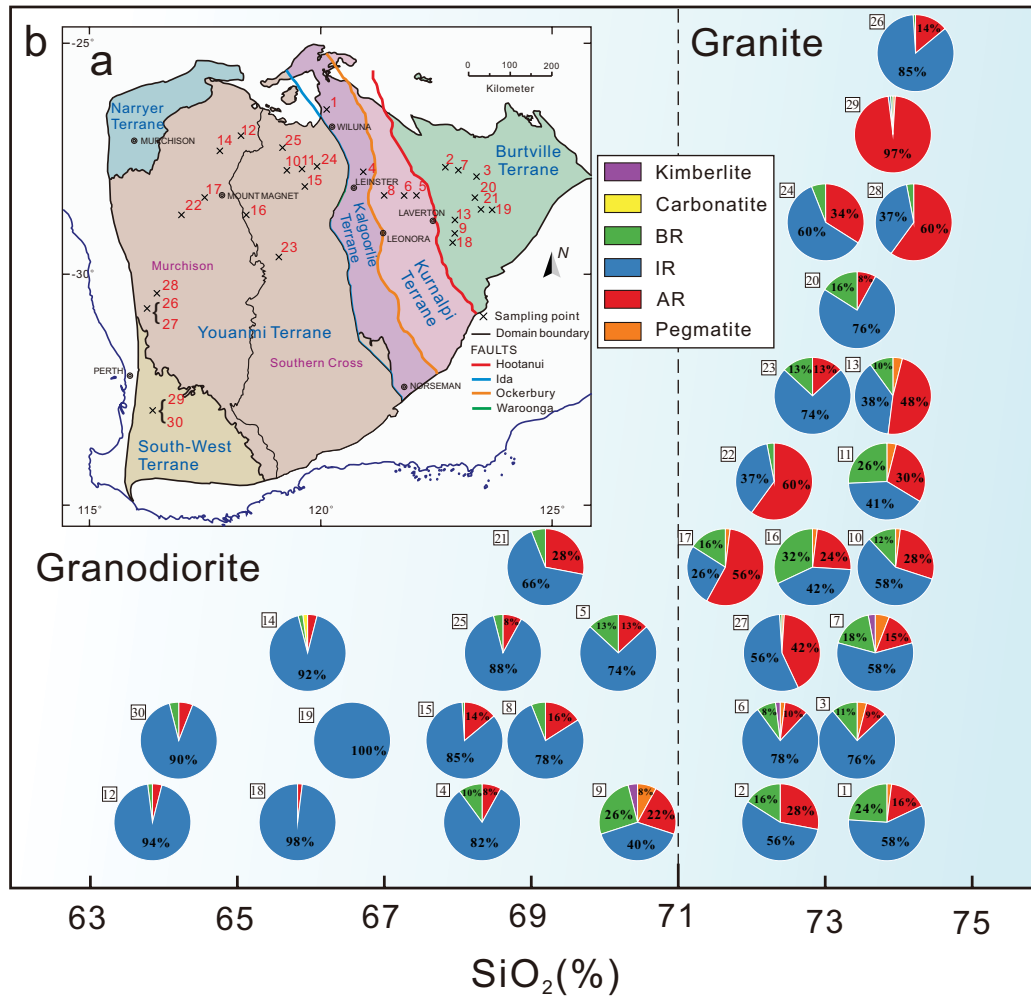
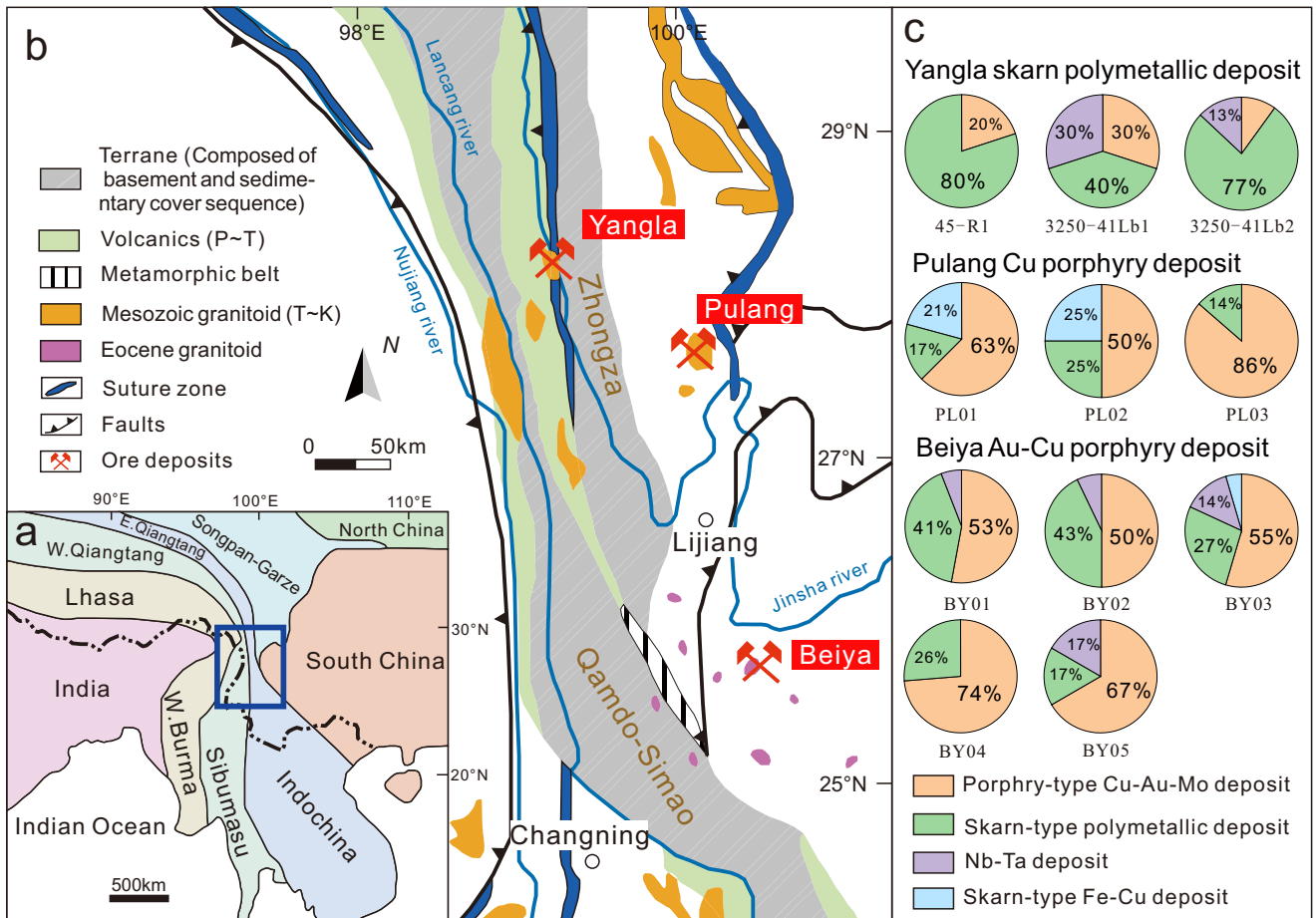


Figure 9





***Table 1 Igneous rock and ore deposit type and data volume***

Database types	Number of publications	Amount of data
<i>Igneous rocks</i>		
Kimberlite	10	549
Carbonatite	8	240
<sup>a</sup> BR Gabbro	30	1058
Basalt		
<sup>b</sup> IR Andesite	72	2514
Diorite		
<sup>c</sup> AR Granite	66	2594
Rhyolite		
Pegmatite	8	218
<i>Deposits</i>		
Porphyry-type Cu-Mo-Au deposit	24	2122
Skarn-type Polymetallic deposit	13	896
Intrusion-related Au deposit	3	203
Skarn-type Fe-Cu deposit	8	529
Nb-Ta deposit	3	81

a. BR - basic rock, include gabbro and basalt;

b. IR - intermediate rock, include andesite and diorite;

c. AR – acid rock, include granite and rhyolite.



**Table 2 Comparison of different data pre-processing strategies and machine learning algorithm**

Algorithm	Data pre-processing strategies			Accuracy
	Missing values filling	Data standardization	Class imbalance	
<i>Igneous rocks classification model (19 features/elements)</i>				
Decision Tree	knn-classification	z-score	smote	0.803
	knn-classification	log	smote	0.798
	knn-classification	minmax	smote	0.790
	iterative	z-score	smote	0.654
	iterative	minmax	smote	0.623
	iterative	log	smote	0.613
XGBoost	knn-classification	minmax	smote	0.870
	knn-classification	z-score	smote	0.868
	knn-classification	log	smote	0.854
	iterative	minmax	smote	0.682
	iterative	z-score	smote	0.689
	iterative	log	smote	0.742
Random Forest	knn-classification	minmax	smote	0.928
	knn-classification	log	smote	0.934
	knn-classification	z-score	smote	0.947
	iterative	z-score	smote	0.805
	iterative	log	smote	0.829
	iterative	minmax	smote	0.828
<i>Ore deposits classification model (17 features/elements)</i>				
Decision Tree	knn-classification	minmax	smote	0.749
	knn-classification	z-score	smote	0.742
	knn-classification	log	smote	0.725
	iterative	minmax	smote	0.533
	iterative	z-score	smote	0.575
	iterative	log	smote	0.591
XGBoost	knn-classification	minmax	smote	0.819
	knn-classification	log	smote	0.807
	knn-classification	z-score	smote	0.799
	iterative	minmax	smote	0.611
	iterative	z-score	smote	0.634
	iterative	log	smote	0.654
Random Forest	knn-classification	z-score	smote	0.856
	knn-classification	log	smote	0.838
	knn-classification	minmax	smote	0.807
	iterative	minmax	smote	0.722
	iterative	z-score	smote	0.704
	iterative	log	smote	0.733

<i>hms</i>	
Performance	
F1-score	Recall
0.833	0.872
0.825	0.861
0.821	0.861
0.661	0.671
0.655	0.718
0.643	0.693
0.892	0.917
0.889	0.914
0.880	0.913
0.713	0.774
0.725	0.781
0.770	0.808
0.902	0.879
0.902	0.876
0.931	0.917
0.810	0.819
0.834	0.842
0.836	0.847
0.762	0.780
0.759	0.783
0.728	0.749
0.567	0.639
0.594	0.642
0.595	0.601
0.827	0.839
0.813	0.824
0.809	0.827
0.662	0.773
0.685	0.792
0.698	0.785
0.872	0.894
0.855	0.878
0.830	0.866
0.737	0.790
0.734	0.799
0.730	0.758

***Table 3 Optimal parameter tuning results for Random Forests***

Parameters	Igneous rocks classification model		Ore deposits classification model	
	19 features	8 features	17 features	8 features
max_depth	100	44	100	13
max_features	0.444	0.572	0.551	0.649
min_samples_leaf	1	1	1	1
min_samples_split	2	2	2	2
n_estimators	300	300	300	163
F1-score	0.963	0.914	0.890	0.877

***Table 4 Results of Random Forest algorithm with five-fold cross validation***

Database name	Fold 1	Fold 2	Fold 3	Fold 4	Fold 5	Fold avg
Igneous rocks	0.9369	0.9611	0.9501	0.9431	0.9427	0.9468
Ore deposits	0.9089	0.8988	0.9100	0.9187	0.8731	0.9019

**Table 5 Case Study - Application of zircon classifier to igneous rocks in Yilgarn Craton**

Rock number	Latitude and longitude	SiO <sub>2</sub> (%) content of rocks	results of whole-rock geochemistry	Predicti	
				Pegmatite	AR
1	-26.02°S, 120.32°E	73.7	granite	2%	16%
2	-27.86°S, 123.23°E	72.52	granite		28%
3	-27.76°S, 123.37°E	73.26	granite	4.3%	8.7%
4	-27.48°S, 121.02°E	68.46	granodiorite		8.3%
5	-27.89°S, 122.01°E	70.21	granodiorite		13%
6	-27.89°S, 121.88°E	72.43	granite	2%	10%
7	-27.35°S, 123.11°E	73.79	granite	5.9%	14.7%
8	-27.95°S, 121.37°E	69.18	granodiorite		16%
9	-28.77°S, 123.03°E	70.43	granodiorite	8%	22%
10	-27.53°S, 119.5°E	73.99	granite	2%	28%
11	-27.43°S, 119.6°E	73.74	granite	3.7%	29.6%
12	-26.75°S, 118.3°E	63.84	granodiorite		4%
13	-28.51°S, 123.02°E	73.8	granite	4%	48%
14	-27.41°S, 117.7°E	65.63	granodiorite		4%
15	-28.21°S, 119.86°E	67.87	granodiorite		14.1%
16	-28.44°S, 118.62°E	72.73	granite	2%	24%
17	-28.05°S, 117.73°E	71.6	granite	2%	56%
18	-29.02°S, 123.05°E	65.81	granodiorite		2%
19	-28.19°S, 123.67°E	66.54	granodiorite		
20	-27.99°S, 123.43°E	73.06	granite		8%
21	-28.19°S, 123.64°E	69.15	granodiorite		28%
22	-28.61°S, 116.85°E	72.3	granite		60.0%
23	-29.38°S, 119.17°E	72.21	granite		13.3%
24	-27.26°S, 119.96°E	72.95	granite		34%
25	-26.91°S, 119.27°E	68.45	granodiorite		8%
26	-31.03°S, 116.62°E	74.47	granite		14.1%
27	-31.03°S, 116.63°E	72.38	granite	1.40%	41.7%
28	-30.92°S, 116.65°E	74.02	granite		60.0%
29	-32.76°S, 116.38°E	73.89	granite	1.10%	96.7%
30	-32.76°S, 116.36°E	64.04	granodiorite		5.9%

Abbreviations: AR - acid rocks; IR - intermediate rocks; BR - basic rocks

on results of zircon composition				Data source
IR	BR	Carbonatite	Kimberlite	
58%	24%			Nelson DR (1998)
56%	16%			Wingate MTD, et al. (2011)
76.1%	10.9%			Wingate MTD, et al. (2011)
81.2%	10.4%			Nelson DR (1997)
73%	13.3%			Nelson DR (1997)
78%	8%		2%	Nelson DR (1997)
58.8%	17.6%		2.90%	Wingate MTD, et al. (2010)
78%	6%			Nelson DR (1997)
40%	26%		4%	Wingate MTD, et al. (2010)
58%	12%			Wingate MTD and Bodorkos S (2007)
40.7%	25.9%			Wingate MTD and Bodorkos S (2007)
94%	2%			Wingate MTD, et al. (2008)
38%	10%			Wingate MTD, et al. (2011)
92%	2%	2%		Wingate MTD, et al. (2011)
84.7%	1.20%			Wingate MTD, et al. (2012)
42%	32%			Wingate MTD, et al. (2015)
26%	16%			Wingate MTD, et al. (2014)
98%				Wingate MTD, et al. (2010)
100.0%				Wingate MTD, et al. (2011)
76%	16%			Wingate MTD, et al. (2009)
66%	6%			Wingate MTD, et al. (2011)
37%	2.90%			Wingate MTD, et al. (2015)
73.3%	13.30%			Nelson DR (2001)
60%	6%			Love GJ, et al. (2006)
88%	4%			Wingate MTD and Bodorkos S (2007)
84.7%	1.2%			Wingate MTD, et al. (2018)
55.6%	1.4%			Wingate MTD, et al. (2018)
37.1%	2.90%			Wingate MTD, et al. (2018)
1.1%	1.10%			McNaughton N. unpublished cited in Lu et al., (2019)
90.6%	3.5%			McNaughton N. unpublished cited in Lu et al., (2019)